MIRD Dose Estimate Report No. 20: Radiation Absorbed-Dose Estimates for ^{111}In- and ^{90}Y-Ibritumomab Tiuxetan

Darrell R. Fisher[1], Sui Shen[2], and Ruby F. Meredith[2]

[1]Radioisotopes Program, Pacific Northwest National Laboratory, Richland, Washington; and [2]Department of Radiation Oncology, University of Alabama at Birmingham, Birmingham, Alabama

Absorbed-dose calculations provide a scientific basis for evaluating the biologic effects associated with administered radiopharmaceuticals. In cancer therapy, radiation dosimetry supports treatment planning, dose-response analyses, predictions of therapy effectiveness, and completeness of patient medical records. In this study, we evaluated the organ radiation absorbed doses from intravenously administered ^{111}In- and ^{90}Y-ibritumomab tiuxetan. **Methods:** Ten patients (6 men and 4 women) with non-Hodgkin lymphoma, cared for at 3 different medical centers, were administered the tracer ^{111}In-ibritumomab tiuxetan and assessed using planar scintillation camera imaging at 5 time points and CT–organ volumetrics to determine patient-specific organ biokinetics and dosimetry. Explicit attenuation correction based on the transmission scan or transmission measurements provided the fraction of ^{111}In-administered activity in 7 major organs, the whole body, and remainder tissues over time through complete decay. Time–activity curves were constructed, and radiation doses were calculated using MIRD methods and implementing software. **Results:** Mean radiation absorbed doses for ^{111}In- and for ^{90}Y-ibritumomab tiuxetan administered to 10 cancer patients are reported for 24 organs and the whole body. Biologic uptake and retention data are given for 7 major source organs, remainder tissues, and the whole body. Median absorbed dose values calculated by this method were compared with previously published dosimetry for ibritumomab tiuxetan and the product package insert. **Conclusion:** In high-dose radioimmunotherapy, the importance of patient-specific dosimetry becomes obvious when the objective of treatment planning is to achieve disease cures, safely, by limiting radiation dose to any critical normal organ to its maximum tolerable value. Compared with the current package insert, we found differences in median absorbed dose by multiples of 24 in the kidneys, 1.8 in the red marrow, 0.65 in the liver, 0.077 in the intestinal wall, 0.30 in the lungs, 0.46 in the spleen, and 0.34 in the heart wall.

Received Aug. 21, 2008; revision accepted Nov. 21, 2008.
For correspondence or reprints contact: Darrell R. Fisher, Radioisotopes Program, Pacific Northwest National Laboratory, 902 Battelle Blvd., P7-27, Richland, WA 99354.
E-mail: dr.fisher@pnl.gov
In collaboration with the SNM MIRD Committee: Wesley E. Bolch, Darrell R. Fisher, Roger W. Howell, Ruby F. Meredith, George Sgouros (Chair), Barry W. Wessels, and Pat Zanzonico
This report was approved by the MIRD Committee on November 13, 2008.
COPYRIGHT © 2009 by the Society of Nuclear Medicine, Inc.

Key Words: ^{90}Y-ibritumomab tiuxetan; Zevalin; ^{111}In-ibritumomab tiuxetan; MIRD dose estimate report; lymphoma; dosimetry; antibody; radiopharmaceutical

J Nucl Med 2009; 50:644–652
DOI: 10.2967/jnumed.108.057331

Ibritumomab tiuxetan (Zevalin; Cell Therapeutics, Inc.) labeled with ^{90}Y or ^{111}In is the first therapeutic radionuclide–antibody conjugate approved by the U.S. Food and Drug Administration (February 2002). Treatment with ^{90}Y-ibritumomab tiuxetan is indicated for patients with relapsed or refractory low-grade, follicular, or CD20+ transformed B-cell non-Hodgkin lymphoma and is approved as part of a therapeutic regimen involving rituximab (Rituxan; Genentech, Inc.). Tiuxetan is the chelator that binds ^{111}In or ^{90}Y to the antibody.

^{111}In-ibritumomab tiuxetan is administered intravenously as a tracer to assess labeled antibody biodistribution and dosimetry, and ^{90}Y-ibritumomab tiuxetan is administered later, intravenously, as the cancer therapy agent. Patient-specific variables influence radiopharmaceutical behavior and, consequently, the organ-absorbed doses from one patient to another. The purpose of this dose estimate report was to calculate the absorbed doses from intravenously administered ^{111}In- and ^{90}Y-ibritumomab tiuxetan for a small population of lymphoma patients and to evaluate the observed variability.

The biokinetics and dosimetry of ^{111}In- and ^{90}Y-ibritumomab tiuxetan were described previously by others (*1–5*), and dose estimates for ^{90}Y and ^{111}In are summarized in the ibritumomab tiuxetan product package insert (*6*). Cremonesi et al. (*7*) recently analyzed and compared dose estimates for ^{90}Y-ibritumomab tiuxetan in 22 patients by 3 different methods. In recommending patient-specific dosimetry with image correction, Cremonesi et al. (*7*) showed that oversimplified dosimetry provides inaccurate information on dose to critical organs that could affect the amount of ^{90}Y administered and the timing of stem cell transplantation. Assié et al. (*8*) also showed the importance of patient-

specific dosimetry by various methods on assessment of dose from ^{90}Y-ibritumomab tiuxetan. Our study analyzes the biokinetics and dosimetry of ^{111}In- and ^{90}Y-ibritumomab tiuxetan in 10 carefully studied patients representing 3 medical centers. In light of prior analyses by other investigators, the objectives of this work were to generate a MIRD Committee dose estimate for ^{111}In- and ^{90}Y-ibritumomab tiuxetan, base the dose estimate on quantitative imaging that accounted for attenuation correction and background correction of the ^{111}In activity in organs, use patient-specific data on organ mass and body weight, and base this dose assessment on nuclear datasets provided in OLINDA-EXM (Vanderbilt University) (*9*), a calculational tool that implements the MIRD schema (*10*). Results of this study are compared with data in the current product package insert and with recently reported studies for the same radiopharmaceutical.

Mean radiation absorbed doses per unit intake by intravenous infusion of ^{111}In-ibritumomab tiuxetan and ^{90}Y-ibritumomab tiuxetan are given in Tables 1 and 2. The biodistribution data, radionuclide nuclear data, and dosimetric assumptions supporting these calculations are presented in this article.

TABLE 1. Radiation Absorbed Doses per Unit Administered Activity from Intravenous Administration of ^{111}In-Ibritumomab Tiuxetan

Target organ	mGy/MBq
Adrenals	0.202 ± 0.041
Brain	0.082 ± 0.020
Breasts	0.080 ± 0.016
Gallbladder wall	0.229 ± 0.059
Lower large intestine	0.130 ± 0.027
Small intestine	0.145 ± 0.027
Stomach wall	0.139 ± 0.028
Upper large intestine wall	0.147 ± 0.027
Heart wall	0.195 ± 0.048
Kidneys	0.315 ± 0.071
Liver	0.467 ± 0.202
Lungs	0.152 ± 0.036
Muscle	0.103 ± 0.021
Ovaries	0.138 ± 0.028
Pancreas	0.199 ± 0.041
Red marrow	0.272 ± 0.065
Osteogenic cells*	0.312 ± 0.050
Skin	0.065 ± 0.015
Spleen	0.464 ± 0.193
Testes	0.175 ± 0.076
Thymus	0.114 ± 0.024
Thyroid	0.098 ± 0.024
Urinary bladder wall	0.113 ± 0.028
Uterus	0.132 ± 0.029
Total body	0.124 ± 0.022

*Bone surfaces.
Data are mean ± SD. Three significant figures do not imply precision of 1 in 1,000.

TABLE 2. Radiation Absorbed Doses per Unit Administered Activity from Intravenous Administration of ^{90}Y-Ibritumomab Tiuxetan

Target organ	mGy/MBq
Adrenals	0.379 ± 0.118
Brain	0.379 ± 0.118
Breasts	0.379 ± 0.118
Gallbladder wall	0.379 ± 0.118
Lower large intestine	0.379 ± 0.118
Small intestine	0.379 ± 0.118
Stomach wall	0.379 ± 0.118
Upper large intestine wall	0.379 ± 0.118
Heart wall	1.08 ± 0.394
Kidneys	2.44 ± 0.610
Liver	3.64 ± 1.389
Lungs	0.761 ± 0.488
Muscle	0.379 ± 0.118
Ovaries	0.379 ± 0.118
Pancreas	0.379 ± 0.118
Red marrow	2.73 ± 0.909
Osteogenic cells*	2.14 ± 0.519
Skin	0.379 ± 0.118
Spleen	4.65 ± 2.327
Testes	2.16 ± 0.842
Thymus	0.379 ± 0.118
Thyroid	0.379 ± 0.118
Urinary bladder wall	0.379 ± 0.118
Uterus	0.379 ± 0.118
Total Body	0.587 ± 0.107

*Bone surfaces.
Data are mean ± SD. Three significant figures do not imply precision of 1 in 1,000.

Radiopharmaceutical

^{90}Y-ibritumomab tiuxetan is an anti-CD20 murine IgG1 κ-monoclonal antibody (ibritumomab) conjugate using the linker-chelator (tiuxetan). The immunoconjugate results from a thiourea covalent bond between ibritumomab and the linker-chelator tiuxetan and has the form (*N*-(2-bis(carboxymethyl)amino)-3-(*p*-isothiocyanatophenyl)-propyl)-(*N*-(2-bis(carboxymethyl)-amino)-2-(methyl)-ethyl)glycine. This 148-kDa antibody conjugate provides a conformationally restricted ligand for trivalent ^{111}In or ^{90}Y (*11*).

The radiopharmaceutical is given to patients using a 2-step treatment scheme. In step 1, unlabeled rituximab (250 mg/m^2) is given intravenously, followed within 4 h by ^{111}In-ibritumomab tiuxetan (185 MBq) for biodistribution assessment. Rituximab induces complement-dependent cytotoxicity, antibody-dependent cell-mediated cytotoxicity, and programmed cell death (apoptosis) (*12*).

According to the product instructions for ibritumomab tiuxetan (*6*), the diagnostic infusion with ^{111}In-ibritumomab tiuxetan is to be imaged at 48–72 h (and possibly at other selected time points over the first 6 d) to establish the uptake and distribution of ibritumomab in the patient. In step 2, on day 7, 8, or 9, unlabeled rituximab (250 mg/m^2) is administered again, followed within 4 h by a therapeutic infusion of ^{90}Y-ibritumomab tiuxetan (14.8 MBq/kg of

body weight, up to 1,184 MBq) (*1*). In this study, blood samples were also collected and counted for ^{111}In activity to determine retention in serum.

Nuclear Data

^{111}In (valence, +3) is cyclotron-produced by the proton irradiation of ^{112}Cd-enriched targets according to the reaction ^{112}Cd(p,2n)^{111}In. ^{111}In decays with a physical half-life ($t_{1/2}$) of 67.3 h by electron capture to stable ^{111}Cd. The physical emission data for ^{111}In used in OLINDA-EXM are shown in Table 3 (*9,13*).

^{90}Y (valence, +2) is obtained from the natural decay of its parent, ^{90}Sr ($t_{1/2}$, 29 y), which is in turn a product of ^{235}U fission in a nuclear reactor. ^{90}Y is separated radiochemically from ^{90}Sr using a series of precipitation and filtration steps (*14*) or using a series of strontium-selective chromatographic columns. ^{90}Y decays with a physical $t_{1/2}$ of 64 h by β(−) emission to stable ^{90}Zr. The physical emission data for ^{90}Y (*9,13*) are shown in Table 4.

MATERIALS AND METHODS

Subjects

For this dose-estimate study, we selected a study population of 10 (6 men and 4 women) non-Hodgkin B-cell lymphoma patients who consented to more extensive quantitative imaging than required by the routine ibritumomab tiuxetan protocol. Patients were the first consecutively entered, with complete data collection, into a multiinstitutional trial sponsored by Biogen Idec, Inc., at the University of Alabama at Birmingham; Stanford University at Palo Alto, California; and the Mayo Clinic in Rochester, Minnesota, during 2002 to 2005. The lymphoma patients had characteristics similar to those included in prior dosimetry studies (*1–5*), from which the ibritumomab tiuxetan package insert data (*6*) were originally obtained: patients had failed 2 or more prior treatment regimens, had adequate organ function, had less than 25% marrow involvement, and had not received prior external-beam radiation to 25% or more of active marrow. No patients in this study showed evidence of human antimouse antibody response at the time of imaging, determined by the double-antigen method (*15*).

TABLE 3. Nuclear Data for ^{111}In

Principal radiation	E_i (keV)*	n_i	Equilibrium dose constant, Δ_i (rad g μCi^{-1} h^{-1})	Equilibrium dose constant, Δ_i (Gy kg Bq^{-1} s^{-1})
Auger electron	2.7	0.98	5.68E−03	4.27E−16
	19.3	0.156	6.41E−03	4.82E−16
Conversion electron	144.6	0.078	2.40E−02	1.80E−15
	167.3	0.0106	3.78E−03	2.84E−16
	170.5	0.00203	7.37E−04	5.54E−17
	171.2	0.000424	1.55E−04	1.16E−17
	218.7	0.0493	2.30E−02	1.73E−15
	241.4	0.00785	4.04E−03	3.03E−16
	244.6	0.00151	7.87E−04	5.91E−17
	245.3	0.000301	1.57E−04	1.18E−17
x-ray	3.1	0.069	4.60E−04	3.46E−17
	23	0.235	1.15E−02	8.64E−16
	23.2	0.443	2.19E−02	1.64E−15
	26.1	0.145	8.06E−03	6.06E−16
γ	171.3	0.902	3.29E−01	2.47E−14
	245.4	0.94	4.91E−01	3.69E−14

*Average electron energies.

E_i = mean energy per particle or photon; n_i = mean number of particles or photons per nuclear transition; Δ_i = mean energy emitted per nuclear transition.

^{111}In has the following properties: physical half-life, 67.3 h; decay constant, 0.0103 h^{-1}; and decay mode, electron capture.

TABLE 4. Nuclear Data for ^{90}Y

Principal radiation	E_i (keV)*	n_i	Equilibrium dose constant, Δ_i (rad g μCi^{-1} h^{-1})	Equilibrium dose constant, Δ_i (Gy kg Bq^{-1} s^{-1})
β	185.6	0.000115	4.55E−05	3.42E−18
	933.7	0.9999	1.99E+00	1.49E−13
Auger electron	2.02	0.000118	5.08E−07	3.81E−20
Conversion electron	1,743	0.000102	3.79E−04	2.84E−17

*Average β-energy.

^{90}Y has the following properties: physical half-life, 64.1 h; decay constant, 0.0108 h^{-1}; and decay mode, β(−).

Antibody

Ibritumomab binds specifically to the CD20 antigen on human B-cell lymphocytes. The CD20 antigen is expressed on more than 90% of B-cell non-Hodgkin lymphomas but is not expressed on hematopoietic stem cells, normal plasma cells, or other normal, nonlymphatic tissues (*16,17*). The CD20 antigen is not appreciably shed from the cell surface and does not internalize on antibody binding (*17*).

Biologic Data

After infusion, ^{111}In- and ^{90}Y-ibritumomab tiuxetan are distributed by circulating blood to the organs and tissues of the body. Over time, the postinfusion uptake, retention, and clearance of radiolabeled antibody in and from the major normal organs (kidneys, liver, lungs, spleen, heart, red marrow, and testes) and the whole body may be measured using nuclear medicine imaging and radiation detection systems (*2*).

We obtained radiolabeled antibody biodistribution data in patients with low- or intermediate-grade non-Hodgkin lymphoma using tracer infusions of ^{111}In-ibritumomab tiuxetan (185 MBq) after 250 mg/m^2 of rituximab. Measurements were made by quantitative imaging at 5 times on each patient to determine the uptake and biologic retention for radiolabeled antibody in the major organs and tissues. Because ^{90}Y is a pure β-emitter, it cannot be imaged accurately or conveniently in the patient. We assumed that the biodistribution of the trace-labeled ^{111}In-antibody represented the biodistribution of ^{90}Y-antibody in the cancer patient.

Quantitative Imaging

Whole-body scans with conjugate views were obtained to assess whole-body and organ activity over time. Conjugate-view scintillation camera images were acquired immediately after

^{111}In-ibritumomab tiuxetan infusion (time, 0), and again at 4–6 h and on days 1, 3, and 6 through a medium-energy collimator in a 256 × 1,024 acquisition matrix using photopeak settings of 172 and 247 keV with 15% windows. Our objective was to measure the ^{111}In radioactivity in organs at each imaging time point. Imageable source organs included the kidneys, liver, lungs, spleen, heart, red marrow, and testes.

Figure 1 shows anterior and posterior views at 4 h, day 3, and day 6 after infusion of a non-Hodgkin lymphoma patient who was imaged using ^{111}In-ibritumomab tiuxetan. These time-sequential images show decreasing radioactivity in normal organs while radioactivity in disease-containing, enlarged lymph nodes becomes increasingly prominent.

Using standard methods for quantitative imaging (*18–21*), we obtained the geometric mean of the planar anterior and posterior counts to determine the ^{111}In activity in each region for which both anterior and posterior images showed activity above background. For the kidneys and testes, in which uptake was often observed only on posterior or anterior images, respectively, only 1 view was used. Images at early times after injection were acquired at a scan speed of 10 cm/min, and later images were acquired at decreasing speeds; the final image was acquired at 5 cm/min. Each patient's position on the imaging table and the vertical positions of the camera detectors were recorded for the first imaging session; the same positions were applied throughout the sequential imaging studies to ensure reproducible detector-to-patient positioning. A calibrated ^{111}In source (1.85 MBq in 10 mL of water) was included at each image session to correct for potential system drift and to convert image region-of-interest (ROI) counts to units of radioactivity (adjusted with size effect). Counts in selected ROIs were corrected for background. The thickness of the background region was equivalent, after accounting for photon attenuation, to the overlapped background tissues in the organ from the anterior and posterior views.

The importance of attenuation correction in quantitative imaging has long been recognized (*20,21*). We obtained attenuation-correction factors using ^{57}Co transmission images, with and without the patient on the imaging table, according to methods previously described (*22*). For example, the attenuation correction factor for the liver was determined by:

$$ACF_{(^{111}In)} = \left[\sqrt{\frac{N_{nopt}}{N_{pt}}}\right]^{\frac{\mu(^{111}In,\,liver)}{\mu(^{57}Co,\,liver)}}, \qquad \text{Eq. 1}$$

where N_{pt} and N_{nopt} represent the liver ROI counts in the ^{57}Co transmission images with and without the patient, respectively. Equation 1 corrects for energy differences between ^{57}Co and ^{111}In. The values for $\mu_{57Co,liver}$ and $\mu_{111In,liver}$ were determined experimentally from liver phantom studies (*22*). We measured the effective μ values individually using organ phantoms for ^{57}Co and ^{111}In rather than merely assuming that the ratio of μ_{111In} to μ_{57Co} was 1.0 for flood sources. Phantom sizes and depths were selected to mimic sizes and depths for the liver, spleen, kidneys, and tumors in patients.

When substantial amounts (>25%) of the right kidney were overlapped by the liver in the planar view, only the left kidney region was quantified, and the result was doubled to estimate the total kidney uptake. Although the mean contribution to the liver from the overlapping right kidney was 1.6% (range, 0.2%−4.5%), the activity of the overlapping portion of the right kidney was excluded. The remainder-tissue activity was the difference between the whole-body activity and the combined activities of all measured organs. The uptake of ^{111}In-labeled antibody was expressed as percentage of administered activity at each imaging time point.

For a source location that can be visualized only in a single view, a previous study suggested that accurate source quantification could be achieved using single-view techniques and an effective point-source method (*20*):

$$A_{Source} = \frac{I_{Source}}{c}\exp(\mu_{eff}d), \qquad \text{Eq. 2}$$

where I_{source} represents the background-corrected counts per second in the source ROI for the single-view image, and μ_{eff} is the effective linear attenuation coefficient determined using a 150-mL phantom for the kidneys and spleen (or 50 mL for the lumbar vertebrae) (*22*). The source depth d is determined from CT images, and c is the camera system calibration factor (counts/s/activity) for that source. Because the image acquisition protocol of this study was similar to that of the original phase I/II ibritumomab tiuxetan trial (*23*), image counts in a scatter window were not collected and thus scatter correction was not applied. Phantom studies used ^{111}In to simulate organ uptake in the presence of ^{111}In background concentrations. With high tissue backgrounds, we found relatively little gain from scatter correction, compared with photon attenuation and background correction.

Organ Volumetrics Using Patient-Specific Measurements

CT images were obtained to associate each patient-specific scintillation camera activity value with a patient-specific organ mass to increase the accuracy of the dose estimate. The liver,

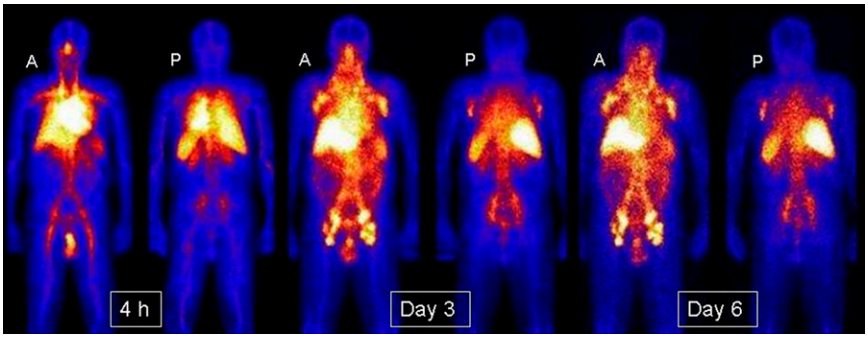

FIGURE 1. Anterior (A) and posterior (P) views of a non-Hodgkin lymphoma patient imaged using ^{111}In-ibritumomab tiuxetan at 4 h, day 3, and day 6 after infusion, showing decrease in normal organ activity over time with increase in lymph node prominence. (Courtesy of the University of Alabama at Birmingham.)

spleen, kidney, and heart volumes were manually defined by individual slice contour drawings on 3- to 5-mm-thick slices. Lung volumes were determined using a contrast-difference edge-detection method with manual correction for air in the main bronchi. A nominal tissue density of 1 g/cm^3 was used for soft tissues except for the lungs, where we assumed the lung density to be 0.26 g/cm^3 (*24*). The heart region was defined as extending below the level in which the pulmonary trunk branches into the left and right pulmonary arteries, because none of the heart chambers extends above the pulmonary arteries. We assumed that the activity measured in the heart was associated with circulating radiolabeled antibody rather than with uptake in the heart muscle. Testicle volumes were not determined because they were out of the CT field of view; red marrow volumes also were not determined. We imaged the second, third, and fourth lumbar vertebral bodies (L2–L4) to directly measure radiolabeled antibody uptake in red marrow space (*25*).

Source Organ Residence Times

We defined a source organ as any organ or tissue for which measurement data were available for calculating internal dose. Decay-corrected measurement data for each source organ, tissue, the whole body, and remainder tissues were converted to percentage administered activity. We plotted the time–activity curves for each source organ in each patient and fit the data using least-squares linear regression to an exponential function. The organ time–activity curves were fit to a single exponential when the correlation coefficient was good ($r \geq 0.98$) but otherwise were fit to a biexponential function. For organs or tissues with delayed uptake followed by exponential clearance, as is typical of the kidneys and testes, we fit the time–activity curves to a biexponential uptake–washout equation:

$$y = (1 - e^{-bx}) + ce^{-dx}, \qquad \text{Eq. 3}$$

where x is time after administration (h). The area under the time–activity curve is proportional to the residence time (Bq-h/Bq), an input value to dosimetry software. Residence times were calculated for the whole body, each source organ, and the remainder tissues by integrating the area under each time–activity curve represented by the best-fit exponential and dividing by the administered activity. The remainder-tissue activity was determined by subtracting the sum of the measured source organ activities from the whole-body activity at each measurement time.

Absorbed-Dose Calculations

The OLINDA-EXM software (*9*) implements the calculational schema recommended by the SNM MIRD Committee (*10*). The residence times based on the ^{111}In measurements and area-under-the-curve analysis for each of the major source organs and remainder were input into OLINDA-EXM to calculate organ-absorbed doses (*9,13*). OLINDA-EXM also allows entry of user-specified organ volumes and patient weights.

RESULTS

Radiation Absorbed Dose per Administered Activity

Radiation absorbed doses per unit administered activity (mGy/MBq ± SD) were calculated for each of the 10 patients. Tables 1 and 2 summarize the mean absorbed doses for 10 lymphoma patients from administered ^{111}In-ibritumomab tiuxetan and ^{90}Y-ibritumomab tiuxetan, respectively. Results in Tables 1 and 2 were reduced to 3 significant figures.

Radiolabeled Antibody Uptake and Retention Half-Times

After infusion, the ^{111}In-labeled antibody distributed via blood circulation to the major organs, tissues, and tumor masses. Table 5 summarizes the measured uptakes soon after infusion and the mean clearance half-times for the major organs or tissues, the remainder tissues, and the whole body from the decay-corrected measurement data. Table 5 also gives the mean residence times calculated from the effective retention data (not decay-corrected) for each source organ, tissue, and the remainder.

Values in Table 5 suggest single exponentials that may be plotted semilogarithmically. Figure 2 shows the data from Table 5 plotted as single lines without error bars to show the relative biodistribution (uptake and retention) of ^{111}In-ibritumomab tiuxetan in the lymphoma patient.

DISCUSSION

Internal radiation doses for ^{111}In- and ^{90}Y-ibritumomab tiuxetan were obtained from data on the biokinetics of trace-labeled ^{111}In-antibody tracer in 10 lymphoma patients. Measurement data were obtained independently at 3 medical centers using scintillation camera acquisitions for 5 time points after administration of ^{111}In-ibritumomab tiuxetan. All patients in this study exhibited normal biodistribution patterns that would allow them to receive a therapeutic infusion of ibritumomab tiuxetan. Altered biodistribution, such as excess uptake in the kidneys (previously demonstrated by others (*26*) in a small percentage of patients), was not observed in this study.

TABLE 5. Biologic (Decay-Corrected) Data for ^{111}In-Ibritumomab Tiuxetan

Site	Fraction initial uptake (±SD)	Retention half-time (h ± SD)	Residence time (h ± SD)
Heart contents	0.0640 ± 0.0212	48.1 ± 15.8	1.18 ± 0.557
Kidneys	0.0262 ± 0.00780	106 ± 45.7	1.40 ± 0.351
Liver	0.145 ± 0.0253	141 ± 76.0	12.9 ± 4.92
Lungs	0.0394 ± 0.0126	46.6 ± 11.7	1.41 ± 0.904
Red marrow	0.146 ± 0.0283	286 ± 347	11.7 ± 4.52
Spleen	0.0417 ± 0.0143	106 ± 56.5	1.63 ± 0.814
Testes	0.00192 ± 0.00133	67.4 ± 6.86	0.163 ± 0.0650
Whole body	1.0	380 ± 162	
Remainder of whole body	0.535 ± 0.0995	>400 (long)	51.8 ± 16.2

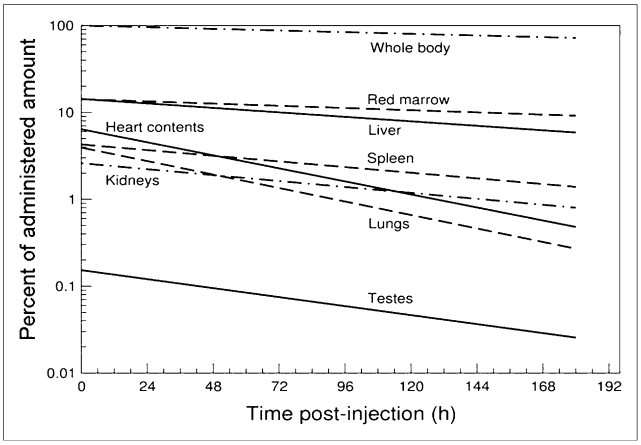

FIGURE 2. Biodistribution of ^{111}In-ibritumomab in whole body and major organs with time after infusion. These decay-corrected (biologic) data plotted semilogarithmically represent mean values for 10 patients in this study (Table 5) to which single-exponential retention functions were applied.

Use of ^{111}In to Predict ^{90}Y Biodistribution

Preclinical studies by others showed that the biodistribution of ^{111}In antibody correlates with ^{90}Y antibody biodistribution (*1,26*). Therefore, it is common practice to use ^{111}In-ibritumomab measurement data to predict the biodistribution of ^{90}Y-ibritumomab. The correlation is only partly correct, however, because partial disassociation of ^{90}Y and ^{111}In from the immunoconjugate may occur in vivo. Some of the free ^{90}Y deposits on bone surfaces, and some of the ^{111}In preferentially goes to the testes because of the uptake of indium by germ cells (*27*). Quality control allowed less than 2% unbound ^{111}In in the injection solution. We did not measure the unbound fraction in serum after injection. For dosimetry calculations, we assumed that the biodistributions of ^{111}In- and ^{90}Y-labeled antibody were equivalent, recognizing that this assumption may lead to underestimates of the ^{90}Y dose to bone surfaces and red marrow and to overestimates of ^{90}Y dose to the testes.

Patient-Specific Organ Mass for Dosimetry

Absorbed dose is inversely proportional to target organ mass. We determined organ masses in each patient for the spleen, liver, kidneys, and lungs by CT. We observed wide variability in organ masses. In lymphoma patients, it is not uncommon for the spleen to be 2–10 times larger than that of the standard reference adult model (183 g). Spleen sizes in these 10 patients ranged from 193 to 697 g (mean ± SD, 369 ± 155 g). Liver sizes ranged from 1,169 to 2,396 g (mean ± SD, 1,679 ± 335 g). Total kidney mass for both kidneys ranged from 221 to 529 g (mean ± SD, 439 ± 99 g). We observed a trend for larger organs in male patients for each organ, with some overlap in values for men and women for all organs except the lungs; female lungs ranged from 2,131 to 4,071 cm^3 (554–1,058 g; mean ± SD, 806 ± 231 g) and male lungs ranged from 4,895 to 6,836 cm^3 (1,273–1,777 g; mean ± SD, 1,633 ± 219 g). Reference values for the 73.7-kg adult (*9*) were assumed for the testes (39.1 g), heart wall (316 g), and red marrow (1,120 g). We assumed that lumbar vertebral regions L2–L4 contained 6.66% of the red marrow mass (*28*).

Limiting Organ Dose

Radiation dose to a critical organ or tissue usually limits the amount of radioactivity that can be safely administered in radioimmunotherapy. Depending on the disease and treatment, critical organs may be the red marrow, liver, lungs, kidneys, stomach, or intestinal tract. We assessed dose to these organs and 18 others and also to the whole body to determine the organ or tissue likely to receive the highest absorbed dose. Radiation absorbed doses reported in this article (Tables 1 and 2) represent the arithmetic average (mean) and SD for each organ and the whole body; the mean is the expectation value of a distribution. We also determined the median values to directly compare our

TABLE 6. Comparison of Median Absorbed Doses per Unit Administered Activity from ^{90}Y-Ibritumomab Tiuxetan for Selected Organs and Tissues

	^{90}Y-ibritumomab tiuxetan absorbed dose (mGy/MBq) in…		
Site	This study	Ibritumomab tiuxetan package insert (online and printed versions (*6*))	Cremonesi et al. (*7*) (method A)
Heart wall	1.0 (0.6–2.0)	2.9 (1.5–3.2)	2.1 (1.1–5.4)
Lungs	0.60 (0.31–1.6)	2.0 (1.2–3.4)	1.7 (0.3–3.5)
Liver	3.1 (2.3–6.6)	4.8 (2.9–8.1)	2.8 (1.8–10.6)
Kidneys	2.4 (1.4–3.9)	0.1 (0.0–0.3)	1.7 (0.6–3.8)
Lower large intestinal wall	0.36* (0.24–0.62)	4.7 (3.1–8.2)	Not reported
Spleen	4.3 (0.98–9.0)	9.4 (1.8–20.0)	1.9 (0.8–5.0)
Red marrow	2.4 (1.7–4.5)	1.3 (0.6–1.8)	0.8 (0.4–1.0)
Testes	1.8 (1.5–3.8)	1.5 (1.0–4.3)	2.8 (1.3–4.7)
Whole body	0.55 (0.44–0.81)	0.5 (0.4–0.7)	0.5 (0.4–0.8)

*Included as 1 of "other organs" or remainder tissues.
Range is presented in parentheses.

results with the estimated absorbed doses provided in the current ibritumomab tiuxetan package insert values (*6*) (Zevalin package insert information is subject to change without notice and is periodically updated by the product manufacturer) and with the results of Cremonesi et al. (*7*), which were published as median and range. The mean and median of a distribution are equivalent if the distribution is normal. For each organ or tissue or the whole body, the absorbed doses in our dataset were found to be lognormally distributed.

In this study, the organs receiving the highest absorbed dose from ^{90}Y-ibritumomab tiuxetan were the spleen (mean, 4.65 mGy/MBq; median, 4.31 mGy/MBq), liver (mean, 3.64 mGy/MBq; median, 3.14 mGy/MBq), and red marrow (mean, 2.73 mGy/MBq; median, 2.39 mGy/MBq). For comparison, the package insert values (*6*) are a median of 9.4 mGy/MBq in the spleen, a median of 4.8 mGy/MBq in the liver, a median of 1.3 mGy/MBq in the red marrow, and a median of 2.4 mGy/MBq in the kidneys. Our results (median values) for these organs were 46% of the current product package insert value for the spleen, 65% of the package insert value for the liver, and 184% of the package insert value for red marrow and 2,400% of the package insert value for the kidneys. In our study, the average lung dose was 0.761 mGy/MBq (median, 0.597 mGy/MBq), which is 30% of the package insert (median) value of 2.0 mGy/MBq.

Cremonesi et al. (*7*) estimated the median absorbed doses for ^{90}Y-ibritumomab tiuxetan using methods (method A: patient-specific organ volumetrics, image correction, and OLINDA-EXM) similar to those used in our study. However, some methods were different: Cremonesi et al. (*7*) calculated red marrow doses using blood concentration data and the method of Sgouros et al. (*29*) to determine the residence times (τ) for marrow, whereas we used the blood data for other purposes and calculated red marrow doses by directly measuring the ^{111}In activity in lumbar vertebral bodies L2–L4 at 5 time points after injection (*25*). We preferred the direct imaging method because marrow uptakes in the lumbar vertebrae were clearly visualized in patients. Table 6 compares the median absorbed doses reported in our study with the current package insert values (*6*) and the values reported by Cremonesi et al. (*7*) for selected organs and tissues and the whole body.

Kidney Dose

In this study, the kidneys received a mean absorbed dose of 2.44 mGy/MBq (median, 2.44 mGy/MBq) from ^{90}Y-ibritumomab tiuxetan. However, the current package insert value (*6*) indicates a dose to the kidneys of 0.1 mGy/MBq. Our median dose for the kidneys is 24.4 times the package insert value (Table 6) but similar to the median dose of 1.7 mGy/MBq reported by others (*7*). The differences may be due to our choice of the kidneys as a source organ, whereas the kidneys were likely assumed to be among the remainder tissues in the package insert studies (*1–5*). Prior dose estimates for ^{111}In-ibritumomab tiuxetan and ^{90}Y-ibritumomab tiuxetan by others may have not fully accounted for photon attenuation; kidney doses were reported to be less than those for the total body, even though activity from kidneys was prominent in the images.

Liver Dose

In this study, we found an average liver dose of 3.64 mGy/MBq (median, 3.1 mGy/MBq) from ^{90}Y-ibritumomab tiuxetan. These values compare (Table 6) with the package insert median of 4.8 mGy/MBq (*6*) and the 2.8 mGy/MBq reported by Cremonesi et al. (*7*).

Lung Dose

In this study, we found an average lung dose of 0.761 mGy/MBq (median, 0.60 mGy/MBq; Table 2) from ^{90}Y-ibritumomab tiuxetan. These values compare (Table 6) with the package insert median of 2.0 mGy/MBq (*6*) and the 1.7 mGy/MBq reported by Cremonesi et al. (*7*). Prior dosimetry studies (*6,7*) assumed a lung mass of 1,000 g (reference man) or 800 g (reference woman) (*9*). Average lung mass in this 10-patient group was 1,182 g, almost 12% greater than the reference man lung mass. Mean photon attenuation in the lungs was 0.60 (range, 0.45–0.73) of the liver attenuation values.

Heart Wall Dose

We calculated a median absorbed dose to the heart wall from circulating ^{90}Y-ibritumomab of 1.01 mGy/MBq. This value is 35% of the dose (2.9 mGy/MBq) given in the ibritumomab tiuxetan package insert (*6*) for ^{90}Y for the heart wall. The differences in absorbed dose to the heart wall reported by others may be due to methods used to evaluate the activity associated with the heart ROI. In our study, we defined the heart activity as a heart ROI, including blood contents, without including major vessels above the pulmonary artery. We also found large variations in heart size. Other investigators may have included a portion of major vessels in their ROI or may not have specifically measured the heart as a major source organ.

Testis Dose

We observed localization of ^{111}In in the testes. None of the patients was known to have testicular disease. Because we had not seen this phenomenon with ^{131}I-labeled antibodies, we attributed the observed uptake to disassociated ^{111}In in testicular germ cells. Direct measurements after an ^{111}In-chloride injection show simple homogeneous biodistribution throughout the body in adults (*27*), together with an enhanced ^{111}In bioconcentration in the testes by a factor of about 3.6. The ^{111}In-ibritumomab tiuxetan uptake and retention half-times that we measured in the testes were more variable from one patient to another than for any other organ in our study.

In the earliest package insert after drug approval, the median ^{90}Y-ibritumomab dose to the testes was reported as 9.1 mGy/MBq and appears to have been a gross overestimate. The testis doses recalculated by the same investigators with different methods resulted in an estimated median

value of 2.8 mGy/MBq, or about a factor of 3 smaller (*2*). Using a background-corrected anterior ROI with attenuation for depth, Shen et al. (*30*) calculated a median testicular dose of 2.4 mGy/MBq, which compares well with the median ^{90}Y testicular dose of 1.8 mGy/MBq and average value of 2.16 mGy/MBq in the present study. Measured uptakes and retention half-times of ^{111}In in the testes were more variable than for other normal organs when studied with ^{111}In-CYT-356, B72.3, and CC49 fusion (*30*–*32*).

Intestinal Wall Dose

We did not observe consistent, measurable uptakes of ^{111}In-ibritumomab in the small or large intestines (*17*). Heterogeneous patches of activity are frequently seen in the bowel, but the activity of these patches has not been readily quantifiable. Such uptake represents Peyer patches (normal lymphoid areas in the bowel) in most patients. Other investigators estimate that about 7% of administered ^{90}Y is excreted in the urine within 10 d and that a lesser amount is excreted in the feces because urinary excretion correlates with decreasing whole-body radioactivity (*6*). Assuming the intestines as remainder tissue and that very little activity cleared in bowel contents, we calculated a median absorbed dose of 0.360 mGy/MBq for the upper large, lower large, and small intestines, in close agreement with a median value of 0.4 mGy/MBq reported by Cremonesi et al. (*7*). Other investigators assigned residence times to activity in the wall of the large intestines (*2*,*24*) rather than to bowel contents, resulting in product package insert values (*6*) of 3.6 mGy/MBq or 4.7 mGy/MBq (depending on the version of insert used).

Whole-Body Dose

In our study, the whole body received a mean absorbed dose of 0.587 mGy/MBq (median, 0.552 mGy/MBq). This result is similar to the current package insert value of 0.5 mGy/MBq (*6*). On average, our results show that a whole-body absorbed dose of 0.75 Gy would be delivered by infusion of about 1.28 GBq of ^{90}Y-ibritumomab tiuxetan.

Effect of Attenuation Correction on Dose Estimation

In the 2001 dosimetry analyses for ibritumomab tiuxetan prepared for regulatory review (*6*), organ and tissue activities were determined using geometric mean ROI counts as a fraction of total counts from the whole body without explicit attenuation correction. This assumption was based on image quantification using a 250-mL source phantom and the baboon liver and spleen (*33*). In our study, we used an explicit attenuation-correction method based on transmission scan or transmission measurement and patient-specific organ masses. To determine the improvement in activity measurement after attenuation correction, we calculated radiation doses to the liver with and without attenuation correction. The overall effect of attenuation correction, compared with the nonattenuated approach, was to reduce the absolute activity in the liver, on average, by a factor of 2.53. For ^{90}Y in the liver, this factor reduced the liver dose by approximately the same factor, showing the overall importance of attenuation correction for internal organ dosimetry.

CONCLUSION

Radiation absorbed-dose calculations provide valuable information for determining the amount of a therapy radiopharmaceutical that may be delivered without exceeding a dose-related toxicity in any normal organ or tissue. This article summarizes the mean and median absorbed doses and compared the medians with values in the current product package insert (*6*) and those reported by Cremonesi et al. (*7*).

We studied the biokinetics and dosimetry of ^{111}In- and ^{90}Y-ibritumomab tiuxetan in 10 patients (6 men and 4 women) with non-Hodgkin lymphoma. We measured the mean initial organ uptake fractions of administered ^{111}In-labeled antibody (at time 0 h) and the mean biologic retention half-times of ^{111}In-labeled antibody in the kidneys, liver, lungs, spleen, heart contents, red marrow, testes, and whole body. The dosimetry was customized using patient-specific quantitative imaging, organ volumetrics from CT scans, and detailed analysis of attenuation factors for several source organs. After integrating the areas represented by the time–activity curves for the major organs, we calculated radiation absorbed doses per unit administered activity for both ^{111}In- and ^{90}Y-labeled antibody in 24 organs and the whole body for each patient. For ^{90}Y, we found that the spleen and liver received the greatest absorbed doses (mean, 4.65 and 3.64 mGy/MBq, respectively). We calculated red marrow doses by measuring the activity in selected lumbar (L2–L4) spaces. The mean absorbed dose to red marrow was 2.73 mGy/MBq, and the mean total-body dose was 0.587 mGy/MBq.

Our dose estimates for the total body and most normal organs are similar to those reported previously by others for various ^{111}In-labeled murine monoclonal antibodies. However, we found substantial differences between our results and the current or previous package insert values. Compared with the current package insert, we found differences in median absorbed dose by multiples of 24 in the kidneys, 1.8 in the red marrow, 0.65 in the liver, 0.077 in the intestinal wall, 0.30 in the lungs, 0.46 in the spleen, and 0.34 in the heart wall.

The wide range of doses calculated for various organs by investigators using patient-specific methods indicates the importance of patient-specific dosimetry for planning and conducting radionuclide therapy procedures. The kidneys and testes are 2 organs of particular interest because of the greater differences in radiation absorbed dose that we found, compared with prior studies, including those doses given in the ibritumomab tiuxetan package inserts. We attribute differences in dose estimates to quantitative imaging techniques and patient-specific organ dosimetry. This work shows that dosimetry approach, assumptions, and choice of parameters can substantially affect the calculated doses. Careful background subtraction, attenuation correc-

tion, use of patient-specific organ masses rather than standard phantom values, and use of updated calculational software can significantly strengthen the overall accuracy of internal radiation dose estimates.

ACKNOWLEDGMENTS

We appreciate the suggestions provided by past MIRD Committee Chair Stephen R. Thomas. Committee tasks are supported by the Society of Nuclear Medicine. We thank Biogen Idec Inc., and specifically Christine A. White and the late Richard Belanger, for permission to use data from protocol UAB 0127 for this analysis. We also thank the protocol principal investigators, Andres Forero (University of Alabama at Birmingham), Gregory A. Wiseman (Mayo Clinic), and Susan J. Knox (Stanford University), who contributed patient data for this study. Manuscript preparation was supported by the U.S. Department of Energy under contract DE-AC05-76RL01830 with Pacific Northwest National Laboratory.

REFERENCES

1. Wiseman GA, Leigh BR, Erwin WD, et al. Radiation dosimetry results from a phase II trial of ibritumomab tiuxetan (Zevalin) radioimmunotherapy for patients with non-Hodgkin's lymphoma and mild thrombocytopenia. *Cancer Biother Radiopharm.* 2003;18:165–178.
2. Wiseman GA, Leigh BR, Erwin WD, et al. Additional radiation absorbed dose estimates for Zevalin radioimmunotherapy. *Cancer Biother Radiopharm.* 2003;18:253–258.
3. Wiseman GA, Kommehl E, Leigh B, et al. Radiation dosimetry results and safety correlations from ^{90}Y-ibritumomab tiuxetan radioimmunotherapy for relapsed or refractory non-Hodgkin's lymphoma: combined data from 4 clinical trials. *J Nucl Med.* 2003;44:465–474.
4. Wiseman GA, Leigh B, Erwin WD, et al. Radiation dosimetry results for Zevalin radioimmunotherapy of rituximab-refractory non-Hodgkin lymphoma. *Cancer.* 2002;94(4, suppl):1349–1357.
5. Wiseman GA, White CA, Sparks RB, et al. Biodistribution and dosimetry results from a phase III prospectively randomized controlled trial of Zevalin radioimmunotherapy for low-grade, follicular, or transformed B-cell non-Hodgkin's lymphoma. *Crit Rev Oncol Hematol.* 2001;39:181–194.
6. Zevalin® prescribing information [package insert]. Seattle, WA: Cell Therapeutics, Inc.; 2008. Available at: www.zevalin.com/pdf/Zevalin_PI_website.pdf. Also available at: http://www.fda.gov/cder/foi/label/2002/ibriide021902LB.pdf. Accessed February 20, 2009.
7. Cremonesi M, Ferrari M, Grana CM, et al. High-dose radioimmunotherapy with ^{90}Y-ibritumomab tiuxetan: comparative dosimetric study for tailored treatment. *J Nucl Med.* 2007;48:1871–1879.
8. Assié K, Dieudonné A, Gardin I, Buvat I, Tilly H, Vera P. Comparison between 2D and 3D dosimetry protocols in ^{90}Y-ibritumomab tiuxetan radioimmunotherapy of patients with non-Hodgkin's lymphoma. *Cancer Biother Radiopharm.* 2008;23:53–64.
9. Stabin M, Sparks RB, Crowe E. OLINDA/EXM: the second-generation personal computer software for internal dose assessment in nuclear medicine. *J Nucl Med.* 2005;46:1023–1027.
10. Loevinger R, Budinger TF, Watson EE. *MIRD Primer for Absorbed Dose Calculations.* Rev ed. Reston, VA: Society of Nuclear Medicine; 1999.
11. Chinn P, Leonard J, Rosenberg J, Hanne N, Anderson D. IDEC-Y2B8: a ^{90}Y-labeled anti-CD20 monoclonal antibody conjugated to MX-DTPA, a high-affinity chelator for yttrium [abstract]. *Proc Am Assoc Cancer Res.* 1999; 40:574.
12. Cartron G, Watier H, Golay J, Solal-Celigny P. From the bench to the bedside: ways to improve rituximab efficacy. *Blood.* 2004;104:2635–2642.
13. Stabin MG, da Luz LC. New decay data for internal and external dose assessment. *Health Phys.* 2002;83:471–475.
14. Bray L, Wester DW, inventors; Battelle Memorial Institute, assignee. Method of separation of yttrium-90 from strontium-90. U.S. patent 5,512,256. April 30, 1996.
15. Khazaeli MB. Quantitation of mouse monoclonal antibody and human anti-mouse antibody response in serum of patients. *Hybridoma.* 1989;8:231–239.
16. Press OW, Appelbaum F, Ledbetter JA, et al. Monoclonal antibody 1F5 (anti-CD20) serotherapy of human B cell lymphomas. *Blood.* 1987;69:584–591.
17. Press OW, Eary JF, Appelbaum FR, et al. Radiolabeled-antibody therapy of B-cell lymphoma with autologous bone marrow support. *N Engl J Med.* 1993;329:1219–1224.
18. DeNardo GL, DeNardo SJ, Macey DJ, Mills SL. Quantitative pharmacokinetics of radiolabeled monoclonal antibodies for imaging and therapy in patients. In: Srivastava SC, ed. *Radiolabeled Monoclonal Antibodies for Imaging and Therapy.* New York, NY: Plenum; 1988:293–310.
19. Eary JF, Appelbaum FL, Durack L, Brown P. Preliminary validation of the opposing view method for quantitative gamma camera imaging. *Med Phys.* 1989;16:382–387.
20. Siegel JA, Thomas SR, Stubbs JB, et al. MIRD pamphlet no. 16: techniques for quantitative radiopharmaceutical biodistribution data acquisition and analysis for use in human radiation dose estimates. *J Nucl Med.* 1999; 40(suppl):37S–61S.
21. Thomas SR, Maxon HR, Kereiakes JG. In vivo quantitation of lesion radioactivity using external counting methods. *Med Phys.* 1976;03:253–255.
22. Shen S, Forero A, LoBuglio AF, et al. Patient-specific dosimetry of pretargeted radioimmunotherapy using CC49 fusion protein in patients with gastrointestinal malignancies. *J Nucl Med.* 2005;46:642–651.
23. Wiseman GA, White CA, Stabin M, et al. Phase I/II ^{90}Y-zevalin (yttrium-90 ibritumomab tiuxetan, IDEC-Y2B8) radioimmunotherapy dosimetry results in relapsed or refractory non-Hodgkin's lymphoma. *Eur J Nucl Med.* 2000;27:766–777.
24. International Commission on Radiological Units and Measurements (ICRU). Tissue Substitutes in Radiation Dosimetry (Report 44). Bethesda, MD: ICRU; 1989. Available at: http://www.icru.org/index2.php?option=com_content&do_pdf=1&id=80. Accessed February 20, 2009.
25. Lim S, DeNardo GL, DeNardo DA, O'Donnell RT, Yuan A, DeNardo SJ. Prediction of myelotoxicity using semi-quantitative marrow image scores. *J Nucl Med.* 1997;38:1749–1753.
26. Conti PS, White C, Pieslor P, et al. The role of imaging with ^{111}In-ibritumomab tiuxetan in the ibritumomab tiuxetan (Zevalin) regimen: results from a Zevalin Imaging Registry. *J Nucl Med.* 2005;46:1812–1818.
27. Nettleton JS, Lawson RS, Prescott MC, Morris ID. Uptake, localization, and dosimetry of ^{111}In and ^{201}Tl in human testes. *J Nucl Med.* 2004;45:138–146.
28. International Commission on Radiological Protection (ICRP). *Report of the Task Group on Reference Man.* ICRP Publication No. 23. Oxford, England: Pergamon Press; 1975.
29. Sgouros G. Bone marrow dosimetry for radioimmunotherapy: theoretical considerations. *J Nucl Med.* 1993;34:689–694.
30. Shen S, Meredith R, Duan J, et al. Testicular uptake and radiation dose in patients receiving Zevalin and Pretarget CC49Fusion protein. *Cancer Biother Radiopharm.* 2005; 20:110–118.
31. Mardirossian G, Brill AB, Harwood SJ, et al. Radiation absorbed dose estimates for indium-111-labeled B72.3, an IgG antibody to ovarian and colorectal cancer: MIRD dose estimate report No. 18. *J Nucl Med.* 1998;39:671–676.
32. Mardirossian G, Brill AB, Dwyer KM, et al. Radiation absorbed dose from indium-111-CYT-356. *J Nucl Med.* 1996;37:1583–1588.
33. van Reenen PC, Lotter MG, Heyns AD, et al. Quantification of the distribution of ^{111}In-labelled platelets in organs. *Eur J Nucl Med.* 1982;7:80–84.